Carbohydrate Polymers 100 (2014) 179–184

Contents lists available at ScienceDirect

Carbohydrate Polymers

journal homepage: www.elsevier.com/locate/carbpol

Cellulose–clay layered nanocomposite films fabricated from aqueous cellulose/LiOH/urea solution

Quanling Yang, Chun-Nan Wu, Tsuguyuki Saito, Akira Isogai*

Graduate School of Agricultural and Life Sciences, The University of Tokyo, 1-1-1 Yayoi, Bunkyo-ku, Tokyo 113-8657, Japan

ARTICLE INFO

Article history:
Received 5 June 2012
Received in revised form 5 October 2012
Accepted 18 October 2012
Available online 26 October 2012

Keywords:
Cellulose
Clay
Montmorillonite
Gas barrier
Nanocomposite

ABSTRACT

Transparent and flexible cellulose–clay (montmorillonite, MTM) nanocomposite films are prepared from cellulose/LiOH/urea solutions. The results show that the composites possess intercalated nanolayered structures. Almost no Na ions are present in MTM, probably because they are substituted by Li ions. The nanocomposite films possess high mechanical strength and gas barrier properties, and lower coefficients of thermal expansion than those of the original cellulose film. In particular, the composite film of 85% cellulose and 15% MTM has the highest tensile strength and Young's modulus 161 and 180% greater than those of the 100% cellulose film, and coefficient of thermal expansion and oxygen permeability at 50–75% RH decrease to 60 and 42–33%, respectively. Moreover, the initial hydrophilic nature of cellulose film changes to somewhat hydrophobic through incorporation of hydrophilic MTM platelets. This is probably because the orientation of cellulose chains on the film surface changes by the formation of numerous hydrogen bonds between cellulose molecules and MTM platelets.

1. Introduction

Recently, understanding and exploiting the unique properties of polymer nanocomposites have received increasing attention (Paul & Robeson, 2008; Svagan et al., 2012; Wang, Cheng, & Tang, 2012). Inorganic films possess higher thermal and chemical resistance as well as a longer lifetime than their polymer counterparts, but they are brittle with poor film-forming ability (Clarizia, Algieri, & Drioli, 2004; Yang & Wang, 2006). In polymer–inorganic nanocomposites, inorganic nanofillers are present in the polymer matrix at almost individual nano-element level and thus nanocomposites behave differently to conventional composites (Braganca, Valadares, Leite, & Galembeck, 2007; Galimberti, Lostritto, Spatola, & Guerra, 2007). Nanocomposites can exhibit a combination of the basic properties of the polymer and inorganic nanofiller, and in some cases offer specific advantages or synergistic properties at particular weight ratios of the two components, such as excellent gas barrier performance, good thermal and chemical resistance and adaptability to harsh environments, while maintaining similar film-forming ability to the original polymer (Lu, Liu, & Duncan, 2003; Tang et al., 2005; Taniguchi & Cakmak, 2004; Zhu, Morgan, Lamelas, & Wilkie, 2001).

Composites of polymers with nanolayered silicates or clays show improved gas barrier, modulus, tensile strength, and thermal stability properties than the polymer alone. The nanolayered platelets of clay form a "tortuous path" for gas molecules in polymer matrices, resembling biomimetic brick and mortar structures (Alexandre & Dubois, 2000; Grunlan, Grigorian, Hamilton, & Mehrabi, 2004; Paul & Robeson, 2008; Ren, Zhu, & Haraguchi, 2011). The addition of nanoclays into polymers has been shown to enhance gas barrier properties relative to the original polymers, and the enhancement is related to the aspect ratio of the nanoclay (Herrera-Alonso, Marand, Little, & Cox, 2009; Paul & Robeson, 2008). Individual clay nanoparticles that can act as gas-impermeable nanoflakes are approximately 1 nm thick, disk-shaped, and possess aspect ratios ranging from 20 to several thousand (Ploehn & Liu, 2006; Priolo, Gamboa, Holder, & Grunlan, 2010; Thompson & Butterworth, 1992; Vali, Hesse, & Kodama, 1992). Polymer–clay nanocomposite materials have been extensively studied since the 1970s (Ebina & Mizukami, 2007; Haraguchi, Ebato, & Takehisa, 2006; Sun, Chu, & Sue, 2010). Sufficient dispersibility of individual nanoclay particles in the polymer matrix is the most significant factor influencing the properties of the composite. However, it is generally difficult to maintain sufficient dispersion of nanoclay particles in composites with high clay loadings. Such clay aggregates cause increased opacity and random platelet alignment that ultimately reduce the gas barrier properties (Kumar et al., 2008; Triantafyllidis, LeBaron, Park, & Pinnavaia, 2006). Thus, incorporation of nanoclay particles into polymeric matrices with high

* Corresponding author. Tel.: +81 3 5841 5538; fax: +81 3 5841 5269.
E-mail address: aisogai@mail.ecc.u-tokyo.ac.jp (A. Isogai).

0144-8617/$ – see front matter © 2012 Elsevier Ltd. All rights reserved.
http://dx.doi.org/10.1016/j.carbpol.2012.10.044

degrees of exfoliation and orientation is currently the most important challenge to fabricate polymer–clay nanocomposites with enhanced properties (Osman, Mittal, Morbidelli, & Suter, 2004; Wu et al., 2012).

Petroleum-based polymers are generally used as matrices in most polymer–clay nanocomposites, and thus are non-biodegradable and not environmentally friendly. New biopolymer materials that are renewable, biocompatible, and biodegradable are in great demand. Cellulose is the most abundant biopolymer on earth, and is attracting renewed interest for materials and energy applications (Cerruti et al., 2008; Klemm, Heubletin, Fink, & Bohn, 2005; Mahmoudian, Wahit, Ismail, & Yussuf, 2012). Regenerated cellulose films prepared from aqueous alkali/urea solutions were found to exhibit good mechanical properties, optical transparency, biocompatibility, biodegradability, and oxygen barrier properties under dry conditions (Cai & Zhang, 2005; Qi, Chang, & Zhang, 2009; Yang, Fujisawa, Saito, & Isogai, 2012; Yang, Fukuzumi, Saito, Isogai, & Zhang, 2011; Yang et al., 2009; Yang, Lue, & Zhang, 2010; Yang, Qin, & Zhang, 2011). However, the oxygen permeability of the cellulose films significantly increased at high humidity (Yang, Fukuzumi, et al., 2011; Yang, Saito, & Isogai, 2012).

In this work, cellulose-based nanocomposite films fabricated from LiOH/urea/cellulose (LUC) solutions were reinforced with natural montmorillonite (MTM) clay particles to improve their mechanical strength, thermal stability and gas barrier properties under humid conditions. The relationships between the nanostructure of clay particles in the cellulose matrix and mechanical, optical, gas-barrier and hydrophilic properties are studied for cellulose–clay nanocomposites with various weight ratios. These cellulose–clay nanocomposites are expected to have superior properties as well as being new eco-friendly materials.

2. Materials and methods

2.1. Materials

A filter paper pulp (highly purified cotton linters, Advantec Co., Ltd., Japan) was used as the cellulose sample with a viscosity-average molecular weight of 8.6×10^4 g mol^{-1} (Yang, Fukuzumi, et al., 2011). Natural MTM with an aspect ratio of 300–600 (Kunipia F, Kunimine Industries Co., Ltd., Japan) was used as the nanoclay sample. The chemical formulae of MTM clay is $Na_{2/3}Si_8(Al_{10/3}Mg_{2/3})O_{20}(OH)_4$, respectively. All reagents and solvents were of laboratory grade and used as received from Wako Pure Chemicals, Tokyo, Japan.

2.2. Preparation of cellulose/MTM composite films

A solution of LiOH/urea/H_2O with a weight ratio of 4.6:15:80.4 was prepared. A desired amount of MTM was dispersed in the above solution, which was then stirred for 2 h at room temperature. The MTM dispersion was further agitated at 7500 rpm for 2 min using a double-cylinder-type homogenizer (Excel Auto ED-4, Nissei, Japan) and then with an ultrasonic homogenizer with a 26 mm probe tip diameter at an output power of 300 W for 6 min (US-300T, Nissei, Japan) at room temperature. The MTM dispersion thus obtained was then cooled to −12 °C in a refrigerator. A desired amount of cellulose was dispersed in the cooled MTM dispersion, which was stirred immediately at 1200 rpm for 10 min to obtain a transparent solution with cellulose content of 4 wt.% (Yang, Fukuzumi, et al., 2011). The blend solution was degassed by centrifugation at 5600 × *g* for 10 min, spread on a glass plate as a 0.5 mm thick layer, and then immersed in acetone at room temperature for 30 min to allow regeneration (Yang, Fukuzumi, et al., 2011). The resulting sheet-like hydrogel was thoroughly washed by soaking in water, fixed on a poly(methyl methacrylate) plate with adhesive tape to prevent shrinkage, and air-dried at ambient temperature.

The weight ratios of cellulose and MTM in the composite films investigated were 100:0, 95:5, 90:10, 85:15 and 80:20, which are denoted LUC, LUC–MTM5, LUC–MTM10, LUC–MTM15 and LUC–MTM20, respectively. In addition, a desired amount MTM was dispersed in deionized water, and the dispersion was stirred and agitated as described above to prepare a 2 wt.% MTM dispersion. The obtained MTM dispersions were dried in a ventilated oven at 40 °C for 3 days to obtain films of MTM.

2.3. Analyses

X-ray diffraction (XRD) patterns of the films were acquired in reflection mode using a RINT 2000 diffractometer (Rigaku, Tokyo, Japan) with monochromator-filtered Cu K_α radiation (λ = 0.15418 nm) at 40 kV and 40 mA. The films were frozen in liquid nitrogen, immediately snapped and then vacuum-dried. The surfaces and cross-sections (fracture surfaces) of the films were coated with osmium using a Meiwafosis Neo osmium coater at 10 mA for 5 s, and observed with a Hitachi S4800 field-emission scanning electron microscope (SEM) at 2 kV. Energy-dispersive X-ray (EDX) analysis of MTM and the composite films was carried out using a Horiba EMAX Energy spectroscope attached to the SEM. In the case of SEM-EDX analysis, the acceleration voltage and accumulation time were set to 10 kV and 500 s, respectively.

The optical transmittance of the films was measured from 400 to 800 nm using a JASCO V-670 UV–Vis spectrophotometer. Tensile tests were performed using a Shimadzu EZ-TEST instrument equipped with a 500 N load cell. Rectangular strips 2 mm × 30 mm in size were cut from the films and tested with a span length of 10 mm at a rate of 1.0 mm min^{-1}. At least 10 measurements were carried out for each sample. The thermal expansion of the films following preheating at 120 °C for 10 min was determined under a load of 0.03 N and a nitrogen atmosphere from 28 to 100 °C at 5 °C min^{-1} using a Shimadzu TMA-60 thermomechanical analyzer.

The rates of oxygen and water vapor transmission of the films were determined at 23 and 37.8 °C, respectively, using a Mocon Ox-Tran Model 2/21MH and Mocon Permatran-W Model 1/50G (Modern Controls Inc., US) under standard conditions (ASTM 3985). Each measurement was continued until the rate of O_2 or water vapor transmission reached a stable value. The gas permeability was calculated from the gas transmission rate and film thickness, and the standard deviations for each film were within ±5%. The film thickness was measured by a micrometer at five points for each sample, and all the films prepared in this study were 30 μm with statistical errors within 3%. The films were conditioned at 23 °C and 50% relative humidity (RH) for 2 days and the moisture contents under these conditions were calculated from the film weights before and after heating at 105 °C for 3 h. The films were immersed in deionized water at room temperature for 6 days to reach swelling equilibrium and water uptakes $W_{(\text{water uptake})}$ were calculated from the film weights before and after heating at 105 °C for 3 h according to the following equation:

$$W_{(\text{water uptake})} = \frac{m_{(\text{wet})} - m_{(\text{dry})}}{m_{(\text{cellulose})}} \times 100\% \quad (1)$$

where $m_{(\text{wet})}$ is the weight of the LUC–MTM film after being immersed in water, $m_{(\text{dry})}$ is the weight of the film after heating, and $m_{(\text{cellulose})}$ is the dry weight of cellulose component in $m_{(\text{dry})}$. Contact angles of water droplets with a volume of 2 μL on the films were measured at 23 °C and 50% RH using a FAMAS DM500 instrument (Kyowa Interface Science Co. Ltd., Japan).

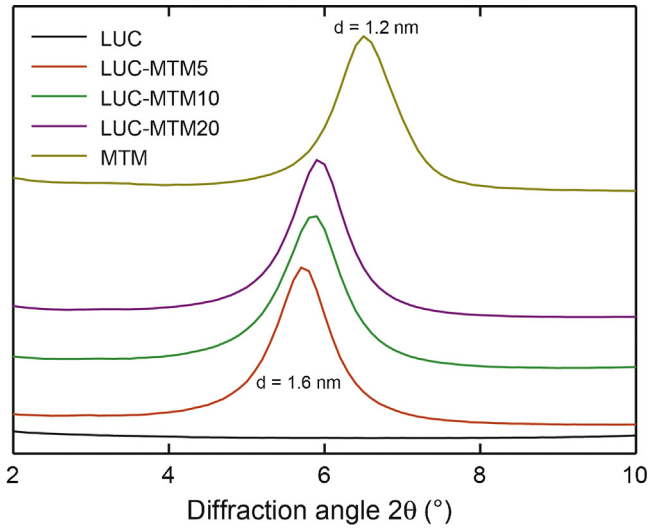

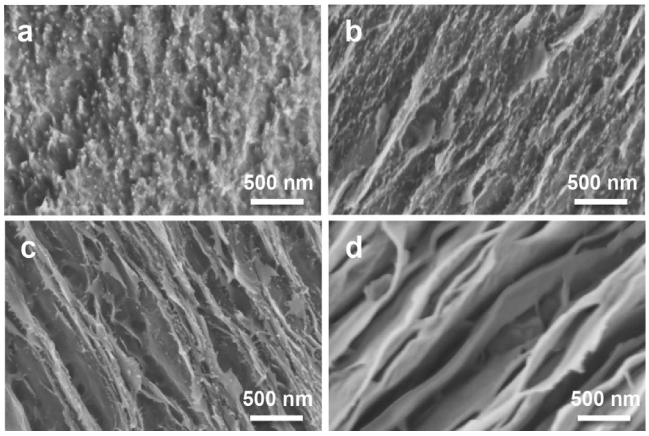

Fig. 1. XRD patterns of LUC, MTM, and LUC–MTM composite films, and SEM images of cross-sections of (a) LUC, (b) LUC–MTM5, (c) LUC–MTM15 and (d) MTM films.

3. Results and discussion

3.1. Structures of cellulose–MTM nanocomposites

The upper graph of Fig. 1 shows XRD patterns of the LUC, MTM, and LUC–MTM composites. The *d*-spacing of (0 0 1) plane of MTM was calculated to be 1.2 nm from the diffraction peak at $2\theta = 6.6^\circ$ using the Bragg equation. LUC has no diffraction peak in the 2θ range from 2° to 10°. The *d*-spacing of MTM increased from 1.2 to 1.6 nm in the LUC–MTM composites as the cellulose content was increased from 0 to 95%, revealing the formation of intercalated structures of MTM platelets in the cellulose matrix films. The *d*-spacing of 1.6 nm for MTM in the LUC–MTM films were 0.4 nm greater than that of the neat MTM film (1.2 nm), which corresponds to the presence of a single layer (ca. 0.4 nm) of cellulose molecules between the MTM platelets (Ebina & Mizukami, 2007; Watanabe & Sato, 1988).

The size of MTM platelets in the planar direction was ~500 nm (Supplementary data, Fig. S1). The SEM images in Fig. 1 show the cross-sections of the films. The MTM films displayed regularly layered platelet structures. Nanolayered structures regularly appeared in the composites with an increase in MTM content, and the layered structures were parallel to the film surface. Meanwhile, the MTM platelets became thinner and displayed smaller interstices as the cellulose content in the composite increased. The XRD and SEM results indicate the formation of intercalated nanolayered platelet structures of MTM in the LUC matrix to form cellulose–MTM nanocomposite films (Wang et al., 2012).

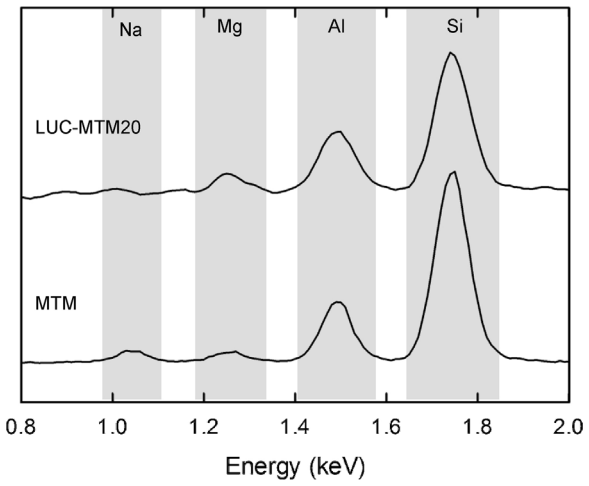

Fig. 2. SEM-EDX patterns of MTM and LUC–MTM20 films.

Because aqueous LiOH/urea solution was used for dissolution of cellulose and dispersion of MTM platelets, it is possible for Na ions in MTM to be exchanged for Li ions in the composites. Fig. 2 shows SEM-EDX patterns of MTM and LUC–MTM20 composite film. As expected, most of the Na ions originally present in MTM were absent from the LUC–MTM20 film. Even though the presence of Li in the composite film could not be directly detected by SEM-EDX analysis because of analytical limitation, it is likely that almost all of the Na ions in the original MTM were substituted for Li ions in the composite. Moreover, such ion-exchange in MTM platelets may enhance the formation of nanolayered structures in LUC–MTM composites.

3.2. Optical and mechanical properties of cellulose–MTM composite films

In general, optical transparency is a useful criterion for the compatibility of composite elements (Krause, 1972). Fig. 3 shows the optical transmittance of the LUC and LUC–MTM nanocomposite films, as well as photograph of LUC–MTM15 film. The photograph shows the good optical transparency and flexibility of the nanocomposite film. The optical transmittance of the LUC film at 600 nm was 90%, and this value decreased to 86–77% for the composites with MTM content of 5–15 wt.%. The optical transmittance

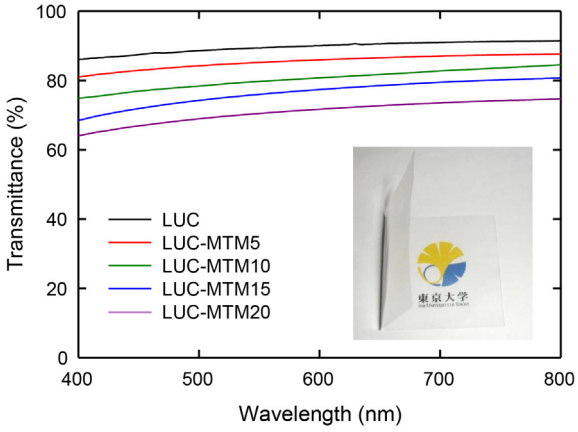

Fig. 3. Visible light transmittance of LUC and LUC–MTM nanocomposite films. Inset shows photograph of LUC–MTM15 film with a thickness of 30 μm.

Table 1
Mechanical properties of LUC and LUC–MTM nanocomposite films.

Sample	Clay content (wt.%)	Tensile strength (MPa)	Young's modulus (GPa)	Elongation at break (%)	Work of fracture (MJ/m^3)
LUC	0	116 ± 21	3.4 ± 0.4	37 ± 9	35.0 ± 2.5
LUC–MTM5	5	160 ± 18	4.7 ± 0.7	29 ± 8	36.9 ± 2.6
LUC–MTM10	10	169 ± 14	5.4 ± 0.9	20 ± 7	26.7 ± 1.5
LUC–MTM15	15	187 ± 11	6.1 ± 0.8	17 ± 6	25.7 ± 2.4
LUC–MTM20	20	161 ± 10	5.1 ± 0.4	14 ± 3	16.9 ± 1.1

of the LUC–MTM nanocomposite films decreased as the content of MTM was increased. It is likely many interfaces are present in the LUC–MTM nanocomposite films, which cause optical scattering and refraction when the content of MTM is high.

The stress–strain curves of the LUC and LUC–MTM nanocomposite films are shown in Fig. S2 of the Supplementary data. The neat MTM film was too brittle to undergo tensile testing. The mechanical properties of the nanocomposite films are listed in Table 1. Young's modulus of the LUC–MTM films increased from 3.4 to 6.1 GPa and the tensile strength increased from 116 MPa to 187 MPa as the MTM content was increased from 0 to 15 wt.%. The work of fracture of the LUC and LUC–MTM films (17–37 MJ m^{-3}) is higher than those of wood (dry yew), steel (spring), bone, rubber (natural), and nanofibrillated cellulose (NFC) paper, which are 0.5, 1, 3, 10 and 15.1 MJ m^{-3}, respectively (Sehaqui, Zhou, & Berglund, 2011). The elongation at break of the LUC–based films was large (14–37% depending on MTM content), so the LUC–MTM nanocomposite films are both highly tough and ductile because of the LUC component. In particular, the LUC–MTM5 film possesses a work of fracture of 36.9 MJ m^{-3} and an elongation at break of 29%. The improvement of these mechanical properties indicates that the MTM platelets are sufficiently dispersed state in the cellulose matrix (Chen & Zhang, 2006; Darder, Colilla, & Ruiz-Hitzky, 2003).

3.3. Thermal properties of cellulose–MTM composite films

The thermal expansion of the films was measured under a nitrogen atmosphere after heating the films at 120 °C for 10 min to remove any residual moisture (Fig. 4). The coefficient of thermal expansion (CTE) of the LUC–MTM nanocomposite films decreased from 18.4 to 11.1 ppm K^{-1} as the MTM content was increased from 0 to 15 wt.%, probably because of the nanolayered structure the MTM platelets. A CTE value of 11.1 ppm K^{-1} was sufficiently low under dry conditions and close to that of glass (~9 ppm K^{-1}) or iron (~11.8 ppm K^{-1}) (Yang, Fujisawa, et al., 2012; Yang, Saito, et al., 2012).

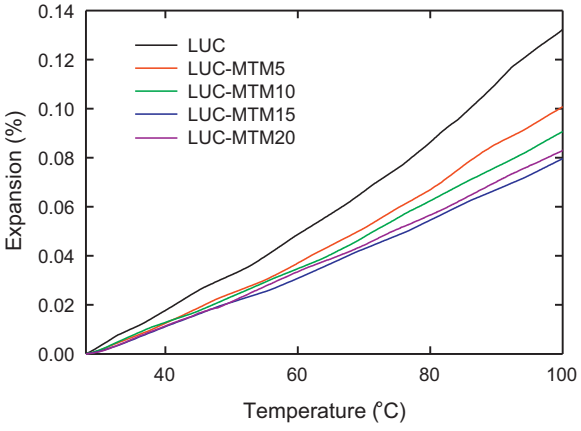

Fig. 4. Thermal expansion behavior of LUC and LUC–MTM nanocomposite films.

3.4. Gas barrier properties of cellulose–MTM composite films

Gas barrier properties of polymer films can be improved by forming composites with inorganic platelets with sufficient aspect ratios, which alter the diffusion path of penetrant gas molecules (Paul & Robeson, 2008). The oxygen transmission rates of the LUC–MTM nanocomposite films at 0% RH were less than 0.0005 mL m^{-2} day^{-1} kPa^{-1}, which was the limit of detection of the instrument. This value is much lower than those of practical oxygen barrier films such as ethylene-vinyl alcohol copolymer, poly(vinylidene chloride), and poly(vinyl alcohol) (Lange & Wyser, 2003). The nanolayered structures of the MTM platelets in the composites should increase the diffusion length for oxygen according to the tortuous-path model (Nielsen, 1967). The original LUC film contains inherently numerous hydrogen bonds formed directly between cellulose molecules under dry conditions, resulting in an extremely low oxygen permeability (Yang, Fukuzumi, et al., 2011).

Fig. 5 shows the oxygen permeabilities of the LUC and LUC–MTM nanocomposite films at 50 and 75% RH. The oxygen permeability of the LUC film was 0.58 and 5.9 mL μm m^{-2} day^{-1} kPa^{-1} at 50 and 75% RH, respectively. The hydrophilic nature of cellulose molecules results in a high moisture content of >10% at 50% RH (Fig. 6), which promotes dissolution and diffusion of oxygen molecules in water molecules absorbed on the LUC film, leading to a significant increase in oxygen permeability (Yang, Fukuzumi, et al., 2011). On the other hand, the oxygen permeability of the LUC film decreased even at 50 and 75% RH upon forming a composite with MTM, again probably owing to the nanolayered structure the MTM platelets.

The oxygen permeabilities of the LUC–MTM nanocomposite films under high RH are comparable to those of practical oxygen barrier films such as poly(vinylidene chloride) (0.4–5.1 mL μm m^{-2} day^{-1} kPa^{-1} at 50% RH), and are much lower than that of high density poly(ethylene) (427 mL μm m^{-2} day^{-1} kPa^{-1} at 50% RH) or poly(ethylene terephthalate) (15.6 mL μm m^{-2} day^{-1} kPa^{-1} at 50% RH) (Miller & Krochta, 1997). The water vapor permeabilities of the LUC film increased with RH, and decreased slightly when composites with MTM were formed (Fig. S3 in the Supplementary data).

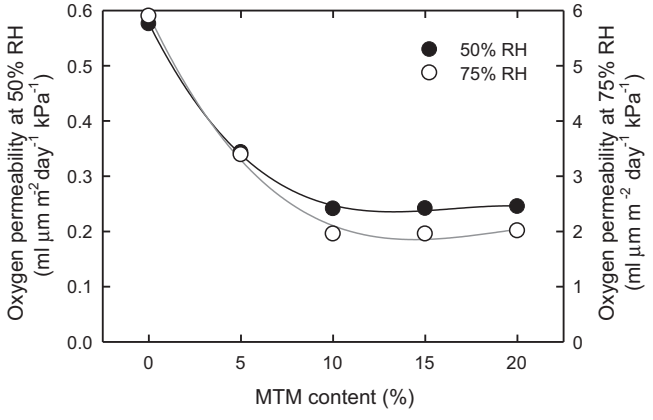

Fig. 5. Oxygen permeabilities of LUC–MTM nanocomposite films at 50% and 75% RH.

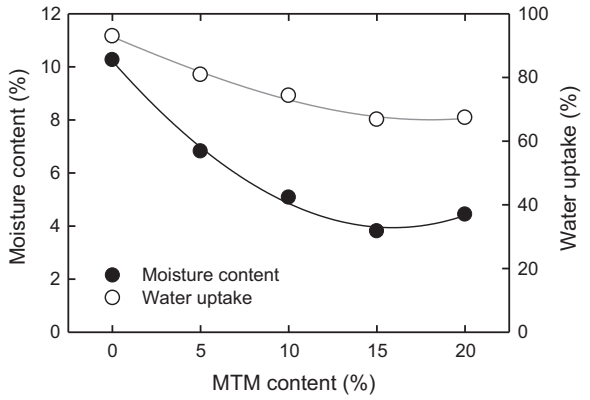

Fig. 6. Effect of MTM content on the moisture content and water uptake of LUC–MTM films. Moisture content was measured after conditioning the films at 23 °C and 50% RH for 2 days. Water uptake was measured after immersing the films in water for 6 days and then calculating the weights of absorbed water and cellulose in the nanocomposites.

3.5. Hydrophilicity of cellulose–MTM composite films

The films were conditioned at 23 °C and 50% RH for 2 days and the moisture contents of the films under these conditions are shown in Fig. 6. The moisture content of the LUC film decreased from 10.3 to 3.8 wt.% when composites containing 15 wt.% MTM were formed. In the next experiment, LUC, MTM, and LUC–MTM nanocomposite films were immersed in water for 6 days to measure water uptake under equilibrium conditions (also shown in Fig. 6). The water uptake of the LUC film decreased from 93 to 67 wt.% when the content of MTM increased from 0 to 15 wt.%.

These decreases in moisture content and water uptake for the nanocomposite films cannot be explained simply by the increased clay content or decrease in the content of hydrophilic cellulose. Thus, the LUC film changed from hydrophilic to hydrophobic when MTM was included. Meanwhile, no weight loss of the LUC or LUC–MTM films was observed after immersion in water for an extended period, showing that the MTM nanoparticles were tightly immobilized in the cellulose matrix, probably by hydrogen bonds. On the other hand, the neat MTM film turned to powder and dispersed during immersion.

Changes in water contact angles on the LUC, MTM, and LUC–MTM nanocomposite films over time are shown in Fig. 7.

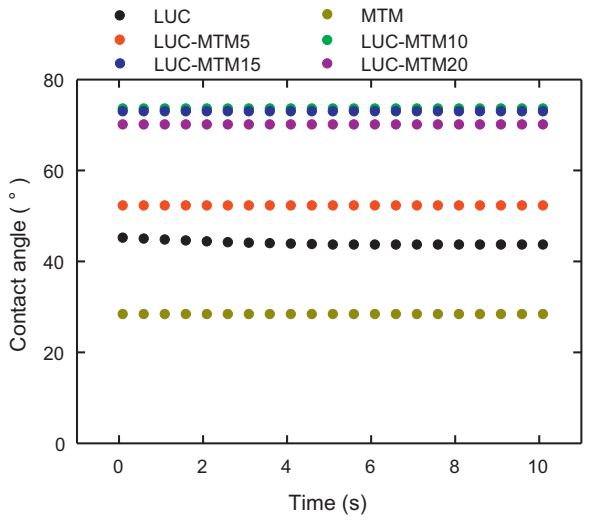

Fig. 7. Changes in the water contact angle on LUC, MTM and LUC–MTM films over time.

Photographs of a water droplet 0.1 s after contact are shown in Fig. S4 of the Supplementary data. The water contact angles of the LUC and MTM film were 45° and 28°, respectively, and remained almost unchanged over time, showing these films are intrinsically hydrophilic. In contrast, the LUC–MTM10 and LUC–MTM15 films had higher water contact angles of ~73°. Thus, the results in Figs. 6 and 7 show that the LUC film changed from hydrophilic to somewhat hydrophobic by addition of 10–20% of MTM. Because each cellulose chain has both hydrophilic OH and hydrophobic CH groups (Yamane et al., 2006), it is likely that predominantly hydrophobic CH groups are present on the surfaces of the LUC–MTM nanocomposite films (Hirota, Tamura, Saito, & Isogai, 2009). Numerous hydrogen bonds formed between cellulose molecules and MTM platelets in the nanocomposites are probably the driving force inducing anisotropic orientation of cellulose chains on the film surfaces.

4. Conclusions

LUC–MTM nanocomposite films fabricated from cellulose/LiOH/urea solutions display high mechanical strength and Young's modulus, and low CTE and oxygen permeability compared with the original LUC film. Formation of regular intercalated nanolayered structures of MTM platelets in the cellulose matrix is likely to have induced such improvements in film properties. In particular, the LUC–MTM15 nanocomposite film had a tensile strength and Young's modulus 161 and 180% greater than those of the LUC film, respectively, and its CTE and oxygen permeability at 50–75% RH were 60 and 42–33% lower, respectively, than those of the LUC film. These effects were attributed to the high aspect ratio of the MTM platelets and their nanolayered structure in the composites. Because the LUC–MTM nanocomposite films have sufficiently large work of fracture and elongation at break, they have high toughness and good ductility. Moreover, the LUC film turns from hydrophilic to somewhat hydrophobic when combined with MTM platelets, probably because the orientation of cellulose chains on the film surface changes in the composites compared with LUC alone.

Acknowledgements

This study was supported by the Japan Society for the Promotion of Science (JSPS): Grant-in-Aid for Scientific Research S (21228007), and Research Fellowships for Young Scientists (24-7663).

Appendix A. Supplementary data

Supplementary data associated with this article can be found, in the online version, at http://dx.doi.org/10.1016/j.carbpol.2012.10.044.

References

Alexandre, M., & Dubois, P. (2000). Polymer-layered silicate nanocomposites: Preparation, properties and uses of a new class of materials. *Materials Science and Engineering*, *28*, 1–63.
Braganca, F., Valadares, L., Leite, C., & Galembeck, F. (2007). Counterion effect on the morphological and mechanical properties of polymer–clay nanocomposites prepared in an aqueous medium. *Chemistry of Materials*, *19*, 3334–3342.
Cai, J., & Zhang, L. (2005). Rapid dissolution of cellulose in LiOH/urea and NaOH/urea aqueous solutions. *Macromolecular Bioscience*, *5*, 539–548.
Cerruti, P., Ambrogi, V., Postiglione, A., Rychlý, J., Matisová-Rychlá, L., & Carfagna, C. (2008). Morphological and thermal properties of cellulose–montmorillonite nanocomposites. *Biomacromolecules*, *9*, 3004–3013.
Chen, P., & Zhang, L. (2006). Interaction and properties of highly exfoliated soy protein/montmorillonite nanocomposites. *Biomacromolecules*, *7*, 1700–1706.
Clarizia, G., Algieri, C., & Drioli, E. (2004). Filler–polymer combination: A route to modify gas transport properties of a polymeric membrane. *Polymer*, *45*, 5671–5681.

Darder, M., Colilla, M., & Ruiz-Hitzky, E. (2003). Biopolymer–clay nanocomposites based on chitosan intercalated in montmorillonite. *Chemistry of Materials*, *15*, 3774–3780.
Ebina, T., & Mizukami, F. (2007). Flexible transparent clay films with heat-resistant and high gas-barrier properties. *Advanced Materials*, *19*, 2450–2453.
Galimberti, M., Lostritto, A., Spatola, A., & Guerra, G. (2007). Clay delamination in hydrocarbon rubbers. *Chemistry of Materials*, *19*, 2495–2499.
Grunlan, J., Grigorian, A., Hamilton, C., & Mehrabi, A. (2004). Effect of clay concentration on the oxygen permeability and optical properties of a modified poly(vinyl alcohol). *Journal of Applied Polymer Science*, *93*, 1102–1109.
Haraguchi, K., Ebato, M., & Takehisa, T. (2006). Polymer–clay nanocomposites exhibiting abnormal necking phenomena accompanied by extremely large reversible elongations and excellent transparency. *Advanced Materials*, *18*, 2250–2254.
Herrera-Alonso, J. M., Marand, E., Little, J. C., & Cox, S. S. (2009). Transport properties in polyurethane/clay nanocomposites as barrier materials: Effect of processing conditions. *Journal of Membrane Science*, *337*, 208–214.
Hirota, M., Tamura, N., Saito, T., & Isogai, A. (2009). Surface carboxylation of porous regenerated cellulose beads by 4-acetamide-TEMPO/NaClO/$NaClO_2$ system. *Cellulose*, *16*, 841–851.
Klemm, D., Heubletin, B., Fink, H. P., & Bohn, A. (2005). Cellulose: Fascinating biopolymer and sustainable raw material. *Angewandte Chemie International Edition*, *44*, 3358–3393.
Krause, S. J. (1972). Polymer compatibility. *Journal of Macromolecular Science, Part C: Polymer Reviews*, *2*, 251–314.
Kumar, S. A., He, Y. L., Ding, Y. M., Le, Y., Kumaran, M. G., & Thomas, S. (2008). Gas transport through nano poly(ethylene-co-vinyl acetate) composite membranes. *Industrial and Engineering Chemistry Research*, *47*, 4898–4904.
Lange, J., & Wyser, Y. (2003). Recent innovations in barrier technologies for plastic packaging—A review. *Packaging Technology and Science*, *16*, 149–158.
Lu, Z. H., Liu, G. J., & Duncan, S. J. (2003). Poly(2-hydroxyethyl acrylate-co-methyl acrylate)/SiO_2/TiO_2 hybrid membranes. *Journal of Membrane Science*, *221*, 113–122.
Mahmoudian, S., Wahit, M. U., Ismail, A. F., & Yussuf, A. A. (2012). Preparation of regenerated cellulose/montmorillonite nanocomposite films via ionic liquids. *Carbohydrate Polymers*, *88*, 1251–1257.
Miller, K., & Krochta, J. (1997). Oxygen and aroma barrier properties of edible films: A review. *Trends in Food Science and Technology*, *8*, 228–237.
Nielsen, L. E. (1967). Models for the permeability of filled polymer systems. *Journal of Macromolecular Science*, *A1*, 929–942.
Osman, M. A., Mittal, V., Morbidelli, M., & Suter, U. W. (2004). Epoxy-layered silicate nanocomposites and their gas permeation properties. *Macromolecules*, *37*, 7250–7257.
Paul, D. R., & Robeson, L. M. (2008). Polymer nanotechnology: Nanocomposites. *Polymer*, *49*, 3187–3204.
Ploehn, H. J., & Liu, C. Y. (2006). Quantitative analysis of montmorillonite platelet size by atomic force microscopy. *Industrial and Engineering Chemistry Research*, *45*, 7025–7034.
Priolo, M., Gamboa, D., Holder, K. M., & Grunlan, J. C. (2010). Super gas barrier of transparent polymer–clay multilayer ultrathin films. *Nano Letters*, *10*, 4970–4974.
Qi, H., Chang, C., & Zhang, L. (2009). Properties and applications of biodegradable transparent and photoluminescent cellulose films prepared via a green process. *Green Chemistry*, *11*, 177–184.
Ren, H., Zhu, M., & Haraguchi, K. (2011). Characteristic swelling–deswelling of polymer/clay nanocomposite gels. *Macromolecules*, *44*, 8516–8526.
Sehaqui, H., Zhou, Q., & Berglund, L. A. (2011). Nanostructured biocomposites of high toughness—A wood cellulose nanofiber network in ductile hydroxyethylcellulose matrix. *Soft Matter*, *7*, 7342–7350.
Sun, D., Chu, C. C., & Sue, H. J. (2010). Simple approach for preparation of epoxy hybrid nanocomposites based on carbon nanotubes and a model clay. *Chemistry of Materials*, *22*, 3773–3778.
Svagan, A. J., Åkesson, A., Caĭrdenas, M., Bulut, S., Knudsen, J. C., Risbo, J., et al. (2012). Transparent films based on PLA and montmorillonite with tunable oxygen barrier properties. *Biomacromolecules*, *13*, 397–405.
Tang, T., Chen, X., Chen, H., Meng, X., Jiang, Z., & Bi, W. (2005). Catalyzing carbonization of polypropylene itself by supported nickel catalyst during combustion of polypropylene/clay nanocomposite for improving fire retardancy. *Chemistry of Materials*, *17*, 2799–2802.
Taniguchi, A., & Cakmak, M. (2004). The suppression of strain induced crystallization in PET through submicron TiO_2 particle incorporation. *Polymer*, *45*, 6647–6654.
Thompson, D. W., & Butterworth, J. T. (1992). The nature of laponite and its aqueous dispersions. *Journal of Colloid and Interface Science*, *151*, 236–243.
Triantafyllidis, K. S., LeBaron, P. C., Park, I., & Pinnavaia, T. J. (2006). Epoxy–clay fabric film composites with unprecedented oxygen-barrier properties. *Chemistry of Materials*, *18*, 4393–4398.
Vali, H., Hesse, R., & Kodama, H. (1992). Arrangement of n-alkylammonium ions in phlogopite and vermiculite; an XRD and TEM study. *Clays and Clay Minerals*, *40*, 240–245.
Wang, J., Cheng, Q., & Tang, Z. (2012). Layered nanocomposites inspired by the structure and mechanical properties of nacre. *Chemical Society Reviews*, *41*, 1111–1129.
Watanabe, T., & Sato, T. (1988). Expansion characteristics of montmorillonite and saponite under various relative humidity conditions. *Clay Science*, *7*, 129–138.
Wu, C.-N., Saito, T., Fujisawa, S., Fukuzumi, H., & Isogai, A. (2012). Ultrastrong and high gas-barrier nanocellulose/clay-layered composites. *Biomacromolecules*, *13*, 1927–1932.
Yamane, C., Aoyagi, T., Ago, M., Sato, K., Okajima, K., & Takahashi, T. (2006). Two different surface properties of regenerated cellulose due to structural anisotropy. *Polymer Journal*, *38*, 819–826.
Yang, Q., Fujisawa, S., Saito, T., & Isogai, A. (2012). Improvement of mechanical and oxygen barrier properties of cellulose films by controlling drying conditions of regenerated cellulose hydrogels. *Cellulose*, *19*, 695–703.
Yang, Q., Fukuzumi, H., Saito, T., Isogai, A., & Zhang, L. (2011). Transparent cellulose films with high gas barrier properties fabricated from aqueous alkali/urea solutions. *Biomacromolecules*, *12*, 2766–2771.
Yang, Q., Lue, A., Qi, H., Sun, Y., Zhang, X., & Zhang, L. (2009). Properties and bioapplications of blended cellulose and corn protein films. *Macromolecular Bioscience*, *9*, 849–856.
Yang, Q., Lue, A., & Zhang, L. (2010). Reinforcement of ramie fibers on regenerated cellulose films. *Composite Science and Technology*, *70*, 2319–2324.
Yang, Q., Qin, X., & Zhang, L. (2011). Properties of cellulose films prepared from NaOH/urea/zincate aqueous solution at low temperature. *Cellulose*, *18*, 681–688.
Yang, Q., Saito, T., & Isogai, A. (2012). Facile fabrication of transparent cellulose films with high water repellency and gas barrier properties. *Cellulose*, http://dx.doi.org/10.1007/s10570-012-9790-5
Yang, Y. N., & Wang, P. (2006). Preparation and characterizations of a new PS/TiO_2 hybrid membranes by sol–gel process. *Polymer*, *47*, 2683–2688.
Zhu, J., Morgan, A. B., Lamelas, F. J., & Wilkie, C. A. (2001). Fire properties of polystyrene–clay nanocomposites. *Chemistry of Materials*, *13*, 3774–3780.